



Chinese Pharmaceutical Association
Institute of Materia Medica, Chinese Academy of Medical Sciences

Acta Pharmaceutica Sinica B

www.elsevier.com/locate/apsb
www.sciencedirect.com



ORIGINAL ARTICLE

Cancer cell membrane-coated bacterial ghosts for highly efficient paclitaxel delivery against metastatic lung cancer



Dandan Ling^{a,b}, Xueli Jia^b, Ke Wang^b, Qiucheng Yan^b,
Bochuan Yuan^b, Lina Du^b, Miao Li^b, Yiguang Jin^{a,b,*}

^aAnhui Medical University, Hefei 230032, China

^bDepartment of Pharmaceutical Sciences, Beijing Institute of Radiation Medicine, Beijing 100850, China

Received 18 April 2023; received in revised form 2 July 2023; accepted 15 July 2023

KEY WORDS

Apoptosis;
Bacterial ghost;
Cancer cell membrane;
Immune stimulation;
Liposome;
Lung targeting;
Metastatic lung cancer;
Paclitaxel

Abstract Chemotherapy is one of the major approaches for the treatment of metastatic lung cancer, although it is limited by the low tumor delivery efficacy of anticancer drugs. Bacterial therapy is emerging for cancer treatment due to its high immune stimulation effect; however, excessively generated immunogenicity will cause serious inflammatory response syndrome. Here, we prepared cancer cell membrane-coated liposomal paclitaxel-loaded bacterial ghosts (LP@BG@CCM) by layer-by-layer encapsulation for the treatment of metastatic lung cancer. The preparation processes were simple, only involving film formation, electroporation, and pore extrusion. LP@BG@CCM owned much higher 4T1 cancer cell toxicity than LP@BG due to its faster fusion with cancer cells. In the 4T1 breast cancer metastatic lung cancer mouse models, the remarkably higher lung targeting of intravenously injected LP@BG@CCM was observed with the almost normalized lung appearance, the reduced lung weight, the clear lung tissue structure, and the enhanced cancer cell apoptosis compared to its precursors. Moreover, several major immune factors were improved after administration of LP@BG@CCM, including the CD4⁺/CD8a⁺ T cells in the spleen and the TNF- α , IFN- γ , and IL-4 in the lung. LP@BG@CCM exhibits the optimal synergistic chemo-immunotherapy, which is a promising medication for the treatment of metastatic lung cancer.

© 2024 The Authors. Published by Elsevier B.V. on behalf of Chinese Pharmaceutical Association and Institute of Materia Medica, Chinese Academy of Medical Sciences. This is an open access article under the CC BY-NC-ND license (<http://creativecommons.org/licenses/by-nc-nd/4.0/>).

*Corresponding author.

E-mail address: jinyg@sina.com (Yiguang Jin).

Peer review under the responsibility of Chinese Pharmaceutical Association and Institute of Materia Medica, Chinese Academy of Medical Sciences.

<https://doi.org/10.1016/j.apsb.2023.08.012>

2211-3835 © 2024 The Authors. Published by Elsevier B.V. on behalf of Chinese Pharmaceutical Association and Institute of Materia Medica, Chinese Academy of Medical Sciences. This is an open access article under the CC BY-NC-ND license (<http://creativecommons.org/licenses/by-nc-nd/4.0/>).

1. Introduction

Cancer is a highly invasive and fatal disease with high morbidity and mortality. The mortality of lung cancer is the first of all cancers with 1.8 million out of 6 million death¹. One common type of lung cancer is metastatic lung cancer due to a number of capillary vessels in the lung, where breast cancer metastatic lung cancer dominates. Chemotherapy of metastatic lung cancer is still the major treatment, though the serious toxicity and side effects are unavoidable^{2,3}. In addition, cancer immunotherapy attracts more and more attention after the CAR-T therapy is applied^{4–6}. Recently, many studies combine chemotherapy and immunotherapy for the treatment of cancers⁷. However, the design of most of them is too complicated to hinder their clinical translation.

Bacterial cancer therapy is initiated by scientists at the beginning of the 19th century⁸. Bacteria-mediated cancer treatment is a hot topic for a long time. The basis of bacterial therapy is the direct action of killing cancer cells and/or the indirect action of stimulating innate and adaptive immune responses with bacteria^{9,10}. Some bacterial vaccines have gone to clinical studies^{11,12}. Conventional bacterial therapy, where natural bacteria are applied, has promising antitumor therapeutic effects, but bacterial toxicity seriously hinders the further application¹³. More recently, the use of genetic engineering to enhance the antitumor activity of bacteria or knockout virulence factors to obtain attenuated bacteria has improved the efficacy and safety of bacterial therapy¹⁴, where the precise expression of bacterial genes *in vivo* is the key. However, there is still a lack of simple and efficient precise manipulation methods. Bacterial therapy has its serious disadvantages where the uncontrollable immune response and subsequent toxicity, such as cytokine storms and sepsis, are difficult to avoid. Therefore, there is no anticancer bacterial formulation in the market even though bacterial therapy has been studied for many years¹⁵. In our previous study, an inhalable bacterial formulation was prepared and intratracheally sprayed into the lung for the treatment of primary lung cancer. A highly efficient anticancer effect was achieved. However, we found that a number of bacteria were present in the important organs such as the heart, which took a huge risk of infections¹⁶. So there is a long route to walk to obtain a successful anticancer bacterial formulation.

Ghosts may be defined the hollow shells from a variety of biological vectors, such as red blood cells, cancer cells, and bacteria, which can be obtained through genetic engineering or fragmentation. They lose their original life characteristics, but retain the corresponding biological characteristics^{17–19}. Bacterial ghosts (BGs) are empty cell envelopes derived from Gram-negative bacteria by bacteriophage ϕ X174 gene E mediated lysis²⁰, which are the hollow shells of bacteria without proliferation function. The controlled expression of ϕ X174 plasmid-encoded lysis gene E in the bacteria is conducted to form transmembrane channels with a diameter of 40–200 nm in the middle or both ends of the bacterial cell membrane, leading to total flowing out of intracellular contents based on the transmembrane osmotic pressure difference²¹. BGs own the complete cell morphology, and more importantly, the antigens, including lipopolysaccharides, lipoproteins, peptidoglycans, and outer membrane proteins, so that they have the function of the immune response of bacteria^{22,23}. BGs provide a possibly safe alternative to toxic bacteria. Moreover, based on their large inner space and complete outer walls, BGs can load a variety of cargoes, such as doxorubicin and ciprofloxacin^{24,25}. Although most of the BGs lose

their flagella, their strong immune stimulation effect is remained due to the presence of lipopolysaccharide and other cell wall components^{26,27}. However, like live bacteria, the safety of BGs is still the key problem for their clinical applications. Cell membrane coating on the surface of BGs is a good method to weaken the immune response of BGs^{28,29}.

Recently, the function of cancer cell membranes (CCMs) attracts attention, which are derived from cancer cell lysis. CCMs were usually used for coating nanoparticles³⁰. CCMs have no genetic transmission risk and are regarded as a novel tumor vaccine. Their homologous affinity function and rich tumor antigens improve tumor cell internalization and personalized immune response. Moreover, the abundant adhesion factors on CCMs mediate the tight junction between homologous tumor cells, contributing to the homologous affinity of tumor tissues^{31–33}. However, the weak immunogenicity of the membrane antigens and the immunosuppressive molecules on the CCM surface hinder the recognition of the immune system, leading to the deficiency of specific immune responses, thus hindering their clinical application^{34–36}. Therefore, it is necessary to combine immune adjuvants to enhance the immune stimulation effect of CCMs.

Here, we designed a series of layer-by-layer encapsulation procedures, where paclitaxel was encapsulated in liposomes to form liposomal paclitaxel (LP), LP was encapsulated in BGs to form LP@BG, and finally LP@BG was encapsulated in CCMs to form LP@BG@CCM (Fig. 1). Only simple encapsulation processes were conducted, involving film formation, electroporation, and extrusion, so that LP@BG@CCM would likely be produced in a large scale. In LP@BG@CCM, the strong immune stimulation of BGs was alleviated by the coating of CCMs, and the tumor cell internalization of CCMs was fully shown. Remarkable antitumor effects were achieved by LP@BG@CCM with the controllable immune response and targeted chemotherapy. The preparation, characteristics, *in vitro* and *in vivo* properties of LP@BG@CCM were explored in this study.

2. Materials and methods

2.1. Materials

Paclitaxel was provided by Fujian South Pharmaceutical Co., Ltd. (Fujian, China). Soybean lecithin (SPC, 90%) and cholesterol were purchased from A.V.T. Pharmaceutical Co., Ltd. (Shanghai, China). Fetal bovine serum (FBS) and Roswell Park Memorial Institute (RPMI 1640) media were purchased from Gibco Life Technologies (Carlsbad, USA). Cell Counting Kit-8 (CCK-8) was purchased from Gen-view Scientific Inc. (El Monte, USA). Membrane and Cytosol Protein Extraction Kit and Antifade Mounting Medium with 4,6-diamino-2-styryl alcohol (DAPI) were purchased from Shanghai Beyotime Biotechnology Co., Ltd. (Shanghai, China). 1,1'-Diiodo-octadecyl-3,3,3',3'-tetramethylindocarbocyanine iodide (DiR), 1,1'-dioctadecyl-3,3,3,3'-tetramethylindocarbocyanine iodide (DiI) and BCA Protein Assay Kit were purchased from Beijing Solarbio Technology Co., Ltd. (Beijing, China). Enzyme-linked immunosorbent assay (ELISA) kits of mouse IL-4, TNF- γ , and TNF- α were purchased from Beijing Neobioscience Biochemical Tech. Co., Ltd. (Beijing, China). Other reagents and excipients were of analytic grade without further purification. Pure water was prepared using Heal Force Super NW Water System (Shanghai Canrex Analytic Instrument Co., Ltd., Shanghai, China).

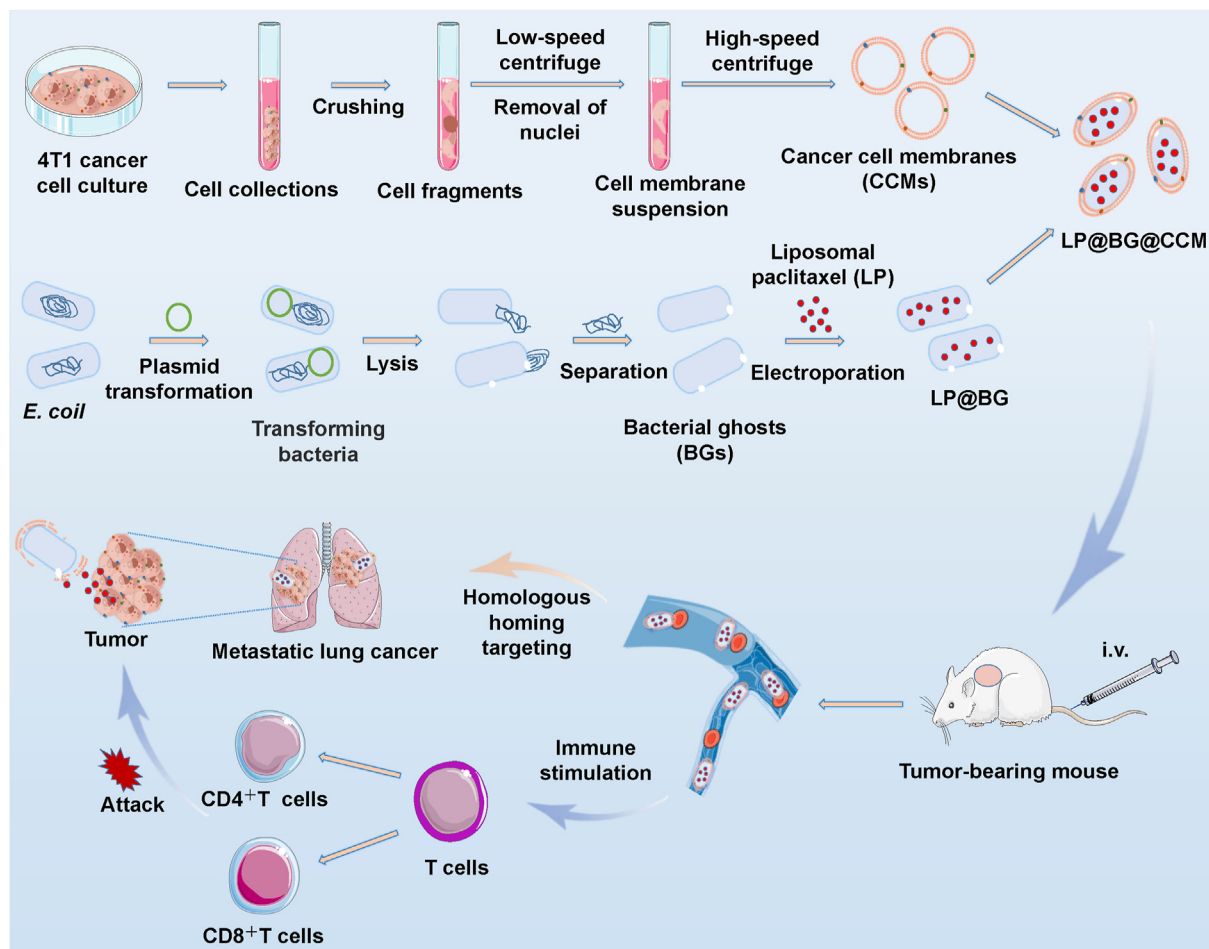


Figure 1 Preparation procedures of LP@BG@CCM and its anticancer mechanism.

2.2. Animals

Female BALB/c mice (19–21 g) were purchased from the SPF Biotechnology Co., Ltd. (Beijing, China). Mice were housed under the constant conditions of humidity ($50 \pm 5\%$) and temperature ($25 \pm 1^\circ\text{C}$) with 12h–12 h light–dark cycles. Food and water were available *ad libitum*. All experimental procedures were approved by the Animal Care and Use Committee of the Beijing Institute of Radiation Medicine and complied with the principles of laboratory animal care and use guidelines.

2.3. Bacteria and cells

Escherichia coli (ATCC 25922) was cultured in Luria–Bertani (LB) media at 37°C . Mouse 4T1 breast cancer cells were purchased from the Cell Bank of the Chinese Academy of Sciences (Shanghai, China) and cultured in the RPMI 1640 supplemented with 10% FBS at 37°C in a humidified 5% CO_2 atmosphere.

2.4. Preparation of BGs

E. coli BGs were manufactured after the controlled expressions of the lysis gene and protein E derived from the phage ϕX174 ¹⁹. Briefly, the pHH43 plasmid containing the phage ϕX174 lysis gene E was introduced into *E. coli* using chemical transformation. *E. coli* containing the plasmid was evenly spread on the surface of

LB agar plates and incubated at 30°C for 32 h to form monoclonal colonies. The monoclonal colonies were selected and transferred to LB liquid media followed by incubation at 28°C in a constant temperature shaker (HNY-200B, Ounuo Instrument Factory, Tianjin, China) until the optical density at 630 nm (OD_{630}) of *ca.* 0.5. The expression of lysis gene E was initiated at 42°C . The OD_{630} of bacterial suspensions was measured every 20 min with a microplate reader (EL \times 800, BioTek Instrument, USA). When the OD_{630} did not decrease, the complete lysis was confirmed. Two types of bacterial suspensions before and after lysis were separately spread on LB agar plates at 30°C overnight to observe the growth of viable bacteria. The lysis efficiency was calculated as in Eq. (1):

$$\text{Lysis efficiency (\%)} = 1 - (\text{Bacteria number after lysis} / \text{Bacterial number before lysis}) \times 100 \quad (1)$$

After comparing the live bacterial numbers of the two types. The lysed bacterial suspension was further treated with gentamicin solutions (0.05 mg/mL) to inactivate possible live bacteria. The suspension was centrifuged with a centrifuge (H2-16 KR, Kecheng Instrument and Equipment Co., Ltd., Changsha, China). The precipitated BGs were washed several times with sterile phosphate-buffered solutions (PBS, pH 7.4), re-suspended in pure water, and lyophilized in a lyophilizer (LGJ-30F, Songyuan Huaxing Technology Develop Co., Ltd., Beijing, China) to get BG powders.

2.5. Preparation of liposomal paclitaxel

Liposomal paclitaxel (LP) was prepared using the film method^{16,37}. Briefly, SPC (0.5 g), cholesterol (50 mg) and paclitaxel (40 mg) were dissolved in absolute ethanol under ultrasound and transferred to a 250-mL round flask. The organic solvent was removed by rotary evaporation under a vacuum, and a film formed at the bottom of the bottle. The film was hydrated with 10 mL of PBS (pH 7.4) in an oscillator at 45 °C for 1 h at 200 rpm until the formation of a homogeneous liposomal suspension.

2.6. Preparation of CCMs

The preparation of CCMs was conducted as the literature³⁸. 4T1 cells were cultured in the RPMI-1640 media containing 10% fetal bovine serum (37 °C, 5% CO₂). When the cells were 80%–90% adherent, 0.25% trypsin was used for digestion followed by centrifugation using a centrifuge (Sorvall Legend Micro 21R, Thermo Fisher Scientific Co., Waltham, USA) at 1000 rpm for 5 min. The cells (5.3×10^8) were washed 2–3 times with the sterile PBS pre-cooled at 4 °C, and the supernatant was withdrawn after centrifugation. The membrane protein extraction reagent A containing 1 mmol/L protease inhibitors was added into the precipitated cells followed by suspending in an ice bath for lysis for 15 min. The suspended cells were disrupted with an ultrasonic cell breaker (HUP-100, Heng Ao Technology Development Co., Ltd., Tianjin, China) and the conditions: 300 W, ultrasound for 5 s, stop for 5 s, repeating 20 times. The suspension was centrifuged at 4 °C and 1000×g for 10 min. The supernatant was collected followed by centrifugation at 4 °C and 21,000×g for 50 min. The precipitated CCMs were collected, suspended in 3 mL of PBS, and stored at –80 °C.

2.7. Preparation of LP@BG

LP-encapsulated BGs (LP@BG) were prepared by electroporation referred to the reference⁴. Briefly, BG powders (20 mg) were dispersed in LP suspensions (2 mL) by vortex for 5 min and transferred into an electric shock cup. The electric shock parameters were set as follows: voltage, 1000 V; electric shock time, 1700–1800 ms; and the number of electric shocks, 10. After the electric shock, the suspension was centrifuged at 4 °C and 1000 rpm for 5 min. The supernatant was discarded and the precipitate was washed 4 times with sterile PBS (pH = 7.4) to remove free liposomes. The precipitate was re-suspended in PBS (3 mL) to obtain LP@BG.

2.8. Preparation of LP@BG@CCM and LP@BG@LM

LP@BG (3 mL) was mixed with a CCM suspension (3 mL) followed by extrusion 15 times through a 1- μ m polycarbonate porous membrane with a liposome micro-extruder (AE001, ATS, Suzhou, China) referred to the literature with modifications³⁹. The extruded suspension was centrifuged at 5000 rpm for 10 min. The supernatant was discarded and the precipitate was re-suspended in PBS (2 mL) to obtain LP@BG@CCM. Blank liposomal membranes (LMs) were prepared according to the method described in LP without adding drugs and LP@BG@LM was prepared with the same method as LP@BG@CCM. In summary, the preparation process of LP@BG@CCM includes three steps: (a) the independent preparation of LP, BGs, and CCMs; (b) the preparation of

LP@BG by electroporation; and (c) the preparation of LP@BG@CCM by extrusion. Every process can be controlled so that the replicability is ensured. The used amounts of components in the preparation of LP@BG@CCM basically kept stable.

2.9. Determination of paclitaxel

Paclitaxel was analyzed with a high-performance liquid chromatographic instrument (HPLC, Agilent 1260, USA) and the following conditions: a Diamonsil C18 ODS column (250 mm \times 4.6 mm, 5 mm), a mobile phase of methanol/water/acetonitrile (40:25:35, v/v) at a flow rate of 1 mL/min, an injection volume of 20 μ L, the detection wavelength of 227 nm, and the column temperature at 30 °C. Lysozyme (20 μ L, 40 mg/mL) was added into LP@BG@CCM (200 μ L). The suspension was incubated in a water bath at 37 °C for 30 min and sonicated at 100 W for 30 min. The suspensions were diluted with methanol and paclitaxel was analyzed by HPLC. Drug loading efficiency was calculated as Eq. (2):

$$\text{Drug loading efficiency (\%)} = \frac{\text{LP@BG@CCM}}{\text{total PTX}} \times 100 \quad (2)$$

2.10. Characterization of formulations

BGs, LP, CCMs, LP@BG, and LP@BG@CCM were stained with a 5% sodium phosphotungstate solution and observed under a transmission electron microscope (TEM, H-7650, Hitachi, Tokyo, Japan). The particle sizes and zeta potentials of them were measured by dynamic light scattering at 25 °C using Zetasizer Nano ZS (Malvern, UK). A carrier formulation containing coumarin-6 liposomes (C6-L) to replace LP and DiI-stained CCMs was prepared to form C6-L@BG@DiI-CCM for simulating LP@BG@CCM. The carrier structure was observed under a confocal laser scanning microscope (CLSM 880, Carl Zeiss AG, Jena, Germany).

2.11. Protein measurement

The proteins of 4T1 cell membranes were measured with the sodium dodecyl sulfate-polyacrylamide gel electrophoresis (SDS-PAGE) method to check whether the proteins were lost in the preparation process referred to the reference⁴⁰. LP, BGs, LP@BG, CCMs, and LP@BG@CCM were collected followed by centrifugation at 4 °C and 5000×g for 10 min. After the removal of the supernatants, an aliquot (0.5 mL) of protein lysates was added, and the proteins were measured with the bicinchoninic acid method. The samples were analyzed with Western blotting.

2.12. Inhibitory effect of cancer cells

4T1 cells (5×10^3 cells/well) were incubated in 96-well plates at 37 °C. When the cell volume reached 80%–90%, the media were replaced with fresh media containing LP, LP@BG, LP@BG@LM, and LP@BG@CCM (containing various concentrations of paclitaxel). The effect of BGs alone was also investigated after BG powders were dispersed in the media with the concentration range of 0.5–0.0625 mg/mL. The cells were incubated for 24 h followed by the addition of 100 μ L of the CCK-8

containing 10% FBS to every well. After incubation for 2 h at 37 °C, OD₄₅₀ was measured using the microplate reader. The cell viability was calculated as Eq. (3):

$$\text{Cell viability (\%)} = (\text{OD}_{\text{sample}} - \text{OD}_{\text{blank}}) / (\text{OD}_{\text{control}} - \text{OD}_{\text{blank}}) \times 100 \quad (3)$$

2.13. Confocal laser scanning microscopy

Confocal laser scanning microscopy (CLSM) was used to detect the cell uptake of C6-L-labelled BGs. 4T1 cells (5×10^4 cells/well) were seeded in confocal small dishes and incubated overnight for adhesion at 37 °C. An aliquot (1 mL) of C6-L, C6-L@BG, C6-L@BG@LM, and C6-L@BG@CCM, all of which contained 5 µmol/L C6, was added to every well, respectively. Three hours later, the media were withdrawn and the cells were washed twice with PBS. DAPI (50 µL, 10 µg/mL) was added to every well followed by incubation for 20 min. An equal (0.1 mL) of the mixture of glycerol/PBS (1:1, v/v) was added to every well. The imaging of cells was conducted using the confocal laser scanning microscope.

2.14. Pharmacodynamic study

Mouse models of metastatic lung cancer were established referred to the literature^{41,42}. Briefly, 4T1 cell suspensions (0.1 mL, 5×10^6 cells/mL) were injected into mice *via* tail veins and they were raised for 5 days (from Day 1 to Day 5) until the lung tumors were formed. The tumor-bearing mice were randomly divided into five groups (4 mice per group) and injected *via* tail veins with 0.2 mL of PBS, BGs, LP, LP@BG, and LP@BG@CCM on Days 6, 9, 12, and 15, respectively. The paclitaxel-contained formulations were intravenously (i.v.) injected with a dose of 10 mg/kg paclitaxel. The mice in the healthy group were not treated. Mice were sacrificed on Day 23. The lungs were excised, photographed, and weighed and the spleens were excised.

2.15. Biodistribution measurement of LP@BG@CCM

An aliquot (1 mL) of CCMs or LMs was mixed with a DiR solution (2 µL, 5 µmol/L) in dimethyl sulphoxide (DMSO) at room temperature for 20 min to obtain DiR-CCMs or DiR-LMs. The labeled membranes were used for the preparation of LP@BG@DiR-LM and LP@BG@DiR-CCM referred to the preparation method of LP@BG@CCM. The tumor-bearing mice were divided into four groups (3 mice per group) and injected with 0.2 mL of PBS, free DiR, LP@BG@DiR-LM, and LP@BG@DiR-CCM, respectively. After the predetermined time intervals (2, 8, 24, 36, and 48 h), the mice were anesthetized with 3% isoflurane and imaged (748/780 nm) using an IVIS *in vivo* system (IVIS[®] Spectrum, PerkinElmer, USA). The mice were sacrificed and the major organ tissues including the heart, liver, spleen, lung, and kidney were excised and imaged. Living Image[®] software (Caliper, Alameda, CA, USA) was used for fluorescence quantification.

2.16. Histopathologic examination

The upper lobes of the right lung were excised and fixed with 4% paraformaldehyde for 24 h, followed by paraffin embedding,

sectioning, and hematoxylin–eosin (H&E) staining. The pathological sections were observed under a microscope (Invitrogen EVOS M5000, ThermoFisher Scientific, USA).

2.17. Immunohistochemistry

The upper lobes of the right lungs were processed as above. The embedded tissues were deparaffined in xylene and rehydrated with ethanol. The standard immunohistochemical process was applied. Briefly, caspase-3 staining was performed according to the instructions and the stained sections were observed under a microscope. TUNEL and DAPI staining were also performed to investigate cell apoptosis.

2.18. ELISA detection

The upper lobes of the left lungs were homogenized using a tissue homogenizer (KZ-II, Wuhan Servicebio Technology Co., Ltd., Wuhan, China) at 60 Hz for 5 min. The homogenates were centrifuged at 5000×g and 4 °C for 10 min and the supernatant was collected for ELISA detection. TNF-α, IL-4, and IFN-γ levels were detected using the ELISA kits (Shanghai Enzyme-linked Biotechnology Co., Ltd., Shanghai, China).

2.19. Distribution of T cell subsets in the spleen

A spleen was transferred to a homogenizing tube and PBS (1 mL) was added to every tube followed by grinding on an ice bath. The homogenates were passed through a 200-mesh screen. The filtrates were collected and red blood cell lysing agents were added followed by incubation for 3 min. The mixture was centrifuged at 1000 rpm and 4 °C for 10 min. The supernatant was withdrawn. The precipitate was re-suspended with the pre-cooled PBS (1 mL) followed by centrifugation as above for 4 times. The final precipitate was suspended with 200 µL of pre-cooled PBS. An aliquot (50 µL) of suspensions was pipetted and diluted with PBS to 1×10^5 – 1×10^8 cells/mL. The diluents were reacted in turn with antigen-presenting cell (APC)-CD4⁺ antibodies and phycoerythrin (PE)-CD8a⁺ antibodies (BioLegend, USA) according to the instructions. The fluorescence was analyzed with a flow cytometer (BD II, BD Biosciences, Franklin Lakes, USA).

2.20. In vivo toxicity assessment

Healthy mice were randomly divided into five groups (3 mice per group) including the PBS, BGs, LP, LP@BG, and LP@BG@CCM groups. The formulations were injected into the mice *via* tail veins, including 0.2 mL of PBS, BGs, LP, LP@BG, and LP@BG@CCM on Days 1, 4, 7, and 10, respectively. The paclitaxel-contained formulations i.v. injected with a dose of 10 mg/kg paclitaxel. On Day 13, the whole blood was collected for serum biochemical analysis of aspartate aminotransferase (AST), alanine aminotransferase (ALT), creatinine (Cr), and creatine kinase (CK). The mice were sacrificed and the major organs were excised and fixed for staining and histopathological examination.

2.21. Data analysis

All data are expressed as mean ± standard deviation (SD). The results were statistically analyzed using GraphPad Prism (Version 8.0, GraphPad Software, LLC). One-way analysis of variance

(ANOVA) was used to determine significant differences between different groups. Statistical difference was considered to be significant when $*P < 0.05$.

3. Results and discussion

3.1. Characteristics of formulations

The mechanism of BG preparation is that the temperature-sensitive pHH43 plasmid expresses and E-lysing proteins are produced over 42 °C, leading to the complete loss of bacterial plasma components and OD₆₃₀ decrease^{43,44}. One key point is incubation time. In this study, the trend of OD₆₃₀ decrease stopped after 120 min (Fig. 2A), indicating that all *E. coli* had been transformed to BGs at this time point and a very high bacterial lysis efficiency of 99.97% was achieved (Fig. 2A). This method can be applied to other Gram-negative bacteria, such as attenuated *Salmonella*²⁰. The isolation of 4T1 CCMs from the cell plasma was confirmed by fluorescence microscopy. The CCMs were stained by DiI (red fluorescence) but not by DAPI (blue fluorescence), while 4T1 cells were stained simultaneously by DiI and DAPI (Fig. 2B). Therefore, no cell plasma was present in the CCMs.

The formulations including LP, CCMs, BGs, LP@BG, and LP@BG@CCM had different morphologies according to their TEM images (Fig. 2C). LP was small sphere-like vesicles and CCMs were large vesicles. The BG-contained formulations including BGs, LP@BG, and LP@BG@CCM showed the bacterial morphology, although LP@BG@CCM had significant coats. The sizes of these formulations showed interesting changes. The sizes of LP and CCMs were 174.23 ± 0.93 and 516.2 ± 24.13 nm ($n = 3$) (Fig. 2D). Whereas, the sizes of the BG-contained formulations were significantly larger than those of LP and CCMs, resulting from the relatively large size of BGs. The sizes of BGs, LP@BG, and LP@BG@CCM were 1369.67 ± 65.59 , 1142.33 ± 61.49 , and 719.23 ± 14.73 nm (Fig. 2E), respectively. The less size of LP@BG@CCM than BGs may result from the repeated extrusion through a filter and some larger particles being held on the filter. In this process, the larger the bacteria were, the easier retention on the filter the bacteria showed. In addition, if the bacteria were not squeezed, the sizes did not change a lot, such as LP@BG vs. BGs.

The C6 and DiI staining experiment further demonstrated their encapsulation relationship. C6-L represented LP and C6-L@BG@DiI-CCM showed the complete BG morphology when C6 fluorescence appeared (Fig. 2F), indicating that C6-L or LP was filled in BGs. C6-L@BG@DiI-CCM showed the basically complete BG morphology when DiI fluorescence appeared and the two types of fluorescent images were merged (Fig. 2D), although a little LP@BG was not coated. Therefore, CCMs were basically completely coated on LP@BG.

The high surface charge of particles, indicated with zeta potentials, enhances the physical stability. Here, the zeta potentials of these formulations clearly showed the cascade encapsulation relationship between them (Fig. 2E). LP had a low zeta potential of -17.03 ± 0.37 mV ($n = 3$). After it was encapsulated into BGs to form LP@BG, its surface charge was covered. The zeta potentials of BGs and LP@BG were very close without statistical difference, *i.e.*, -35.5 ± 1.35 mV and -33.5 ± 1.31 mV, respectively. Similarly, the zeta potentials of CCMs and LP@BG@CCM were also very close without statistical difference, *i.e.*, -26.93 ± 0.54 mV and -27.27 ± 0.85 mV, respectively, meaning that the surface charge of LP@BG@CCM was

determined by CCMs. Moreover, the zeta potentials of LP@BG and LP@BG@CCM had statistical difference ($P < 0.001$). Therefore, we may conclude the coating of CCMs in LP@BG@CCM was basically complete.

CD47 proteins are expressed on the surface of cancer cells, which are considered as a receptor protecting cancer cells from the host immune system^{45,46}. CD44 proteins are a glycoprotein on the cell surface with high expression in malignant tumors, which participate in cell–cell interaction, cell adhesion, and cell migration^{45,46}. LP had no proteins, although BGs and LP@BG had very weak protein bands and CCMs and LP@BG@CCM had remarkable protein bands (Fig. 2G). Moreover, LP, BGs, and LP@BG had no CD47 and CD44 protein expressions and CCMs and LP@BG@CCM had significant expressions (Fig. 2H). Therefore, the marker proteins of CCMs, including CD47 and CD44, were kept in LP@BG@CCM.

3.2. Highly efficient *in vitro* anticancer effect of LP@BG@CCM

LP@BG showed a higher anticancer effect than LP in the investigated paclitaxel concentration range (1–8 μmol/L), indicating the synergistic effect of LP and BGs. BGs could improve LP entering cells. To demonstrate the function of BGs, LP@BG was coated with conventional lipid membranes (LMs) to form LP@BG@LM. Interestingly, the *in vitro* anticancer effect of LP@BG@LM was significantly lower than that of LP@BG. LM should shield the BGs, weakening the cell internalization enhancement function of BGs. But when 4T1 cancer cell membranes, *i.e.*, CCMs, became the outermost membranes of the formulation, *i.e.*, LP@BG@CCM, the highest anticancer effect appeared in the investigated paclitaxel concentration range (Fig. 3A). The 8 μmol/L paclitaxel-loaded LP@BG@CCM almost completely inhibited the growth of 4T1 cells. The strong affinity of CCMs with their donor cells, *i.e.*, 4T1 cells, should mainly contribute to the enhancement effect.

The fluorescence-labeled experiment further demonstrated the above result. C6-L, simulating LP, basically appeared on the surface of 4T1 cells when co-incubation (Fig. 3B). C6-L@BG, simulating LP@BG, improved the cell internalization of C6-L with significant fluorescence in the cell plasma. However, C6-L@BG@LM, simulating LP@BG@LM, mainly remained in the surface of 4T1 cells, similar to C6-L alone. In fact, C6-L or LP had the same membrane components as LMs, including phospholipid and cholesterol molecules. Therefore, the cell internalization of ordinary lipid vesicles was weak. Other studies also demonstrate this result⁴⁷. When LMs were replaced with CCMs to form C6-L@BG@CCM, the new formulation was prone to cell internalization due to the homologous affinity effect.

3.3. High *in vivo* antitumor effect of LP@BG@CCM by improving immune responses and cancer cell apoptosis

A mouse model of metastatic lung cancer was established 6 days after 4T1 cells were *i.v.* injected into the mice (Fig. 4A). On Day 23, the lungs of the model group were tumid with many tumor nodes and hemorrhage compared to the smooth and pink lungs of healthy mice (Fig. 4B). Moreover, the lung volume and weight of the lungs of the model group were much larger than the healthy lungs (Fig. 4B and C). The average lung weight (812.5 ± 31.12 mg) of the model group was even more than three times of that (250 ± 14.14 mg) of the healthy group. In contrast, the average lung weight (327.5 ± 30.31 mg) of the

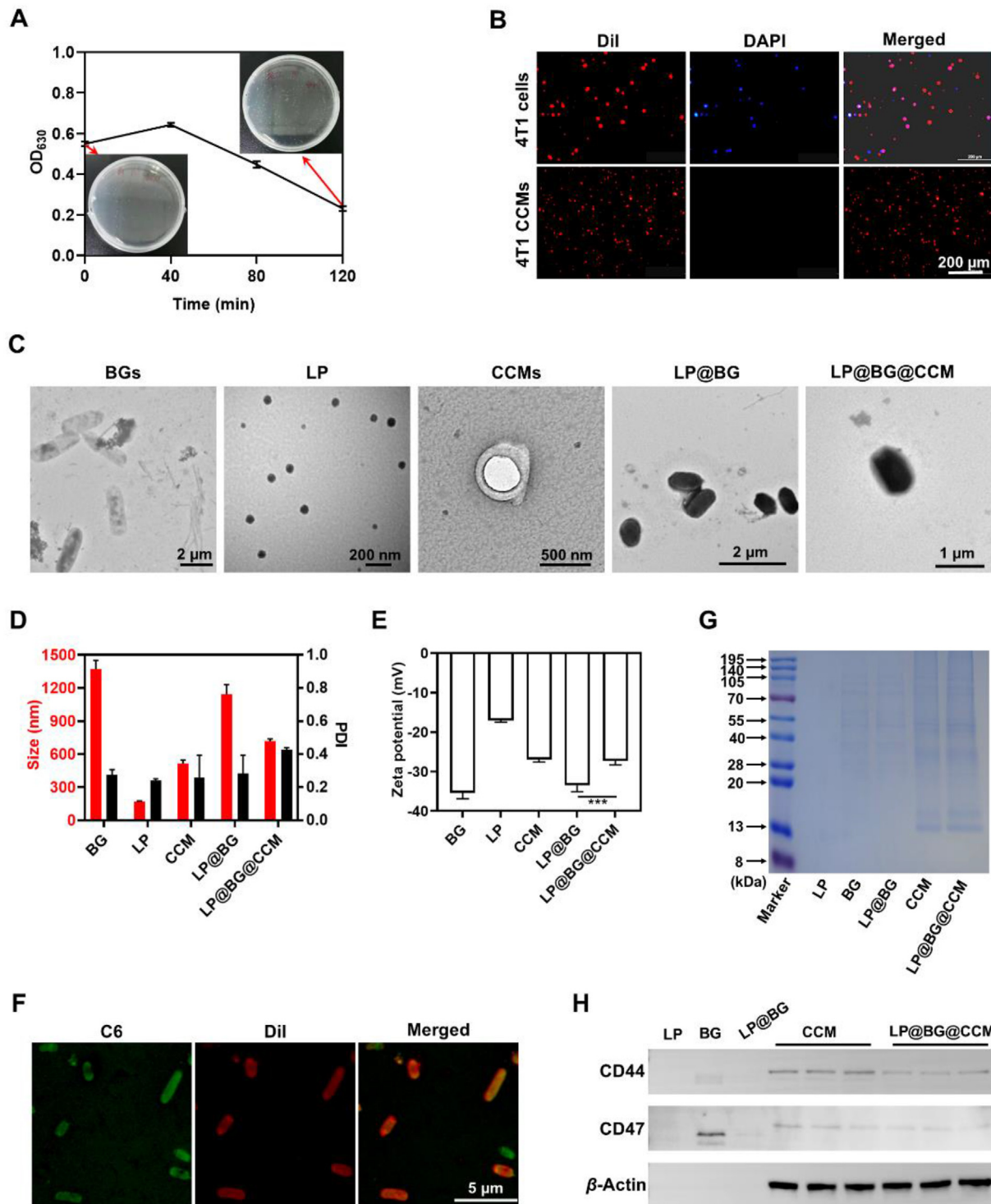


Figure 2 Characteristics of BGs, LP, CCMs, LP@BG, and LP@BG@CCM. (A) OD₆₃₀ of *E. coli* suspensions, where the inset pictures indicate the incubation situation before bacterial lysis (10^5 dilutions for samples) and after bacterial lysis for 120 min (10 dilutions for samples). (B) Microscopic images of the 4T1 cells and the 4T1 cell membranes after DiI (red) and DAPI (blue) staining. (C) TEM images of the formulations. (D) Particle size distribution and PDI, and (E) the zeta potentials of the formulations. Data are presented as mean \pm SD ($n = 3$). (F) CLSM images of C6-L@BG@DiI-CCM with DiI-labeled CCMs (red) and C6-L (green). (G) Protein SDS-PAGE images of the formulations. (H) Western-blotting images of CD47 and CD44 proteins. *** $P < 0.001$.

LP@BG@CCM group had no statistical difference with that of the healthy group (Fig. 4C). The lung appearance of the BG-treated mice was similar to that of the model mice (Fig. 4B),

indicating that BGs alone should have no anticancer effect. After treatment with LP or LP@BG, the lung appearance was remarkably modified and the lung volume and weight were significantly

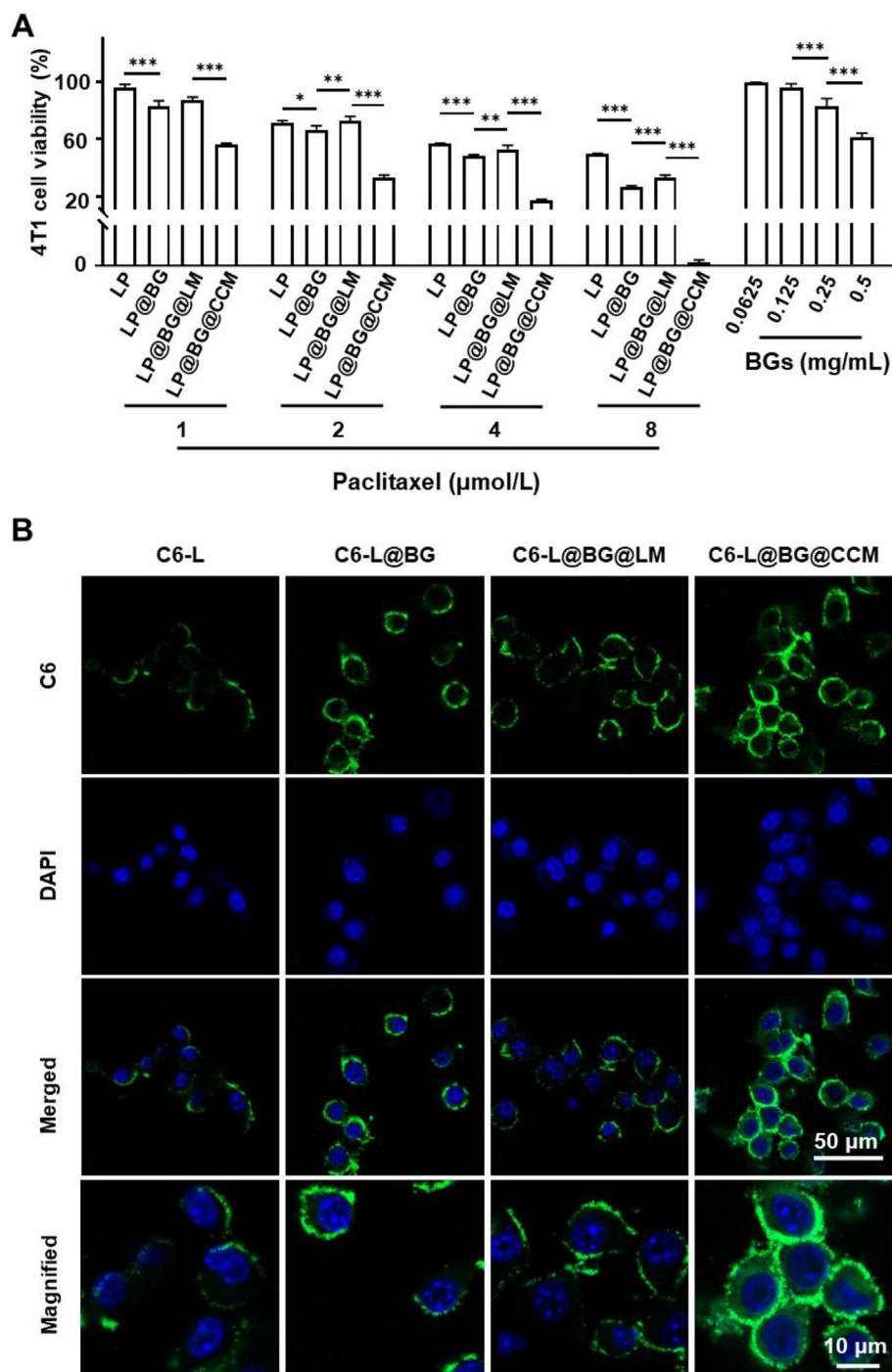


Figure 3 Cytotoxicity and CLSM images. (A) Effects of the coating layers on the viability of 4T1 cells depending on paclitaxel concentrations and formulations. Data are presented as mean \pm SD ($n = 4$). * $P < 0.05$, ** $P < 0.01$, *** $P < 0.001$. (B) CLSM images of various formulations after 3 h incubation with 4T1 cancer cells.

lower than those of the healthy mice (Fig. 4B and C). More importantly, the treatment with LP@BG@CCM made the lung appearance and weight close to the normal state of healthy mice (Fig. 4B and C), indicating the very strong antitumor effect of LP@BG@CCM. Moreover, the H&E stained images of the lung tissue sections further the strong antitumor effect of LP@BG@CCM (Fig. 4D). Dense cancer cells were observed in the tumor tissues and a great deal of infiltrating inflammatory cells appeared. Once cancer cells invaded the whole lung, its respiratory

function would be severely weakened, leading to death. The BG group had similar pathological sections to the model group. The LP and LP@BG groups showed significantly modified lung structures compared to the model group (Fig. 4D). As the above results, the lung structures of the LP@BG@CCM-treated mice had been greatly modified.

Apoptosis is an important factor in cancer cell death. The expression of TUNEL and Caspase-3 can show the state of apoptosis⁴⁸. In this study, the TUNEL and Caspase-3 stained lung

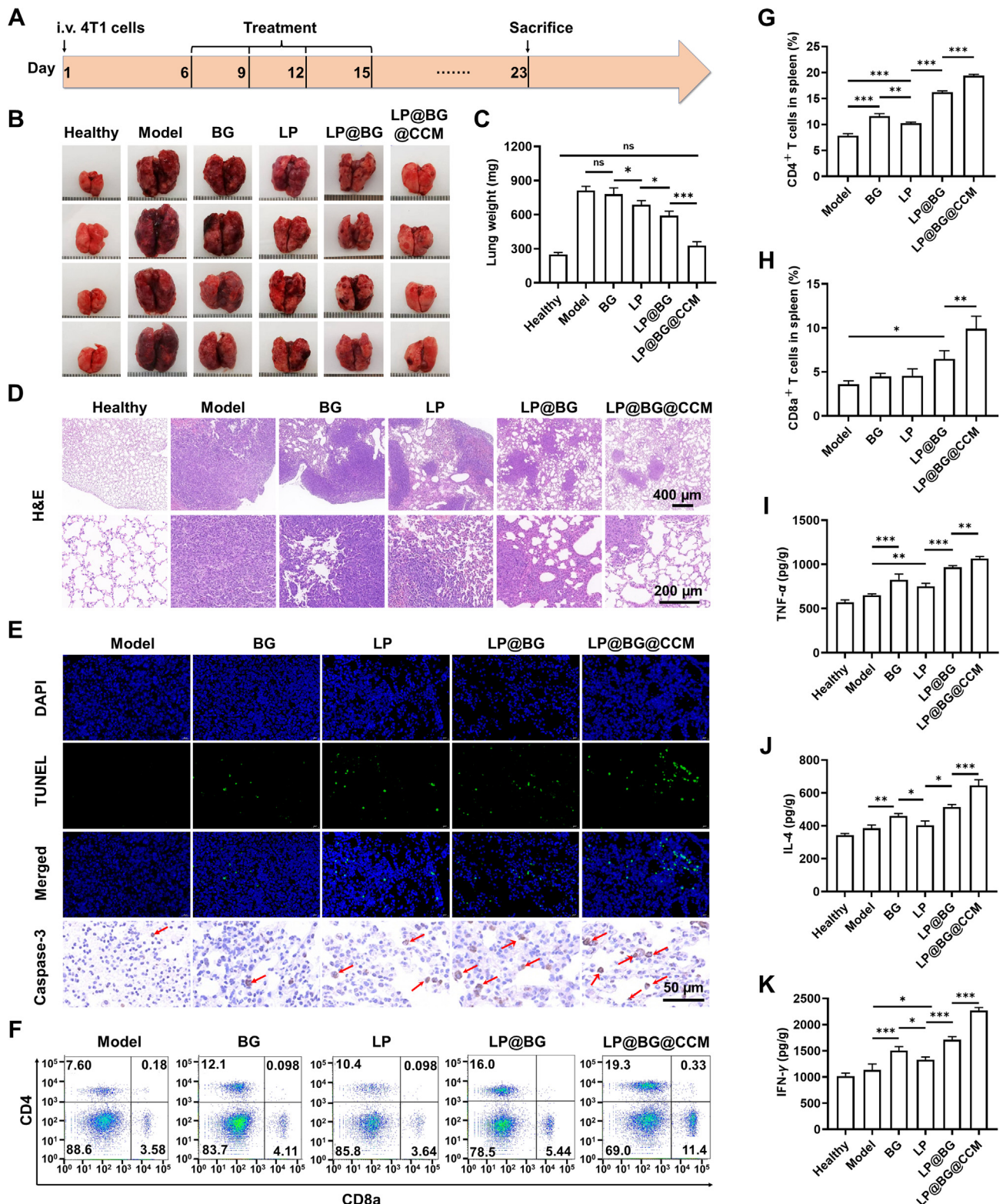


Figure 4 Antitumor effects of formulations. (A) Experimental procedure of the pharmacodynamic study. (B) Appearance and (C) the weight of the lungs of the various groups. (D) H&E and (E) TUNEL and caspase-3 stained images of the lung tissue sections of the various groups. (F) FACS graphs of the CD4⁺ T cells and CD8a⁺ T cells in the spleens. The numbers in the four fields are the percentage of cells. Quantitative analysis of (G) CD4⁺ T cells and (H) CD8a⁺ T cells in the spleens ($n = 3$). Levels of (I) TNF- α , (J) IL-4, and (K) IFN- γ of the lung tissues ($n = 4$). * $P < 0.05$, ** $P < 0.01$, *** $P < 0.001$.

tissue sections showed that BGs had a little antitumor effects (Fig. 4E). LP and LP@BG had significant antitumor effect though the latter's effect was a little more. Therefore, the strong anticancer effect of chemotherapy was confirmed. Moreover, LP@BG@CCM had a much stronger apoptosis effect than the other formulations, which was regarded as the synthetic effect of the components of this system.

We detected the immune stimulations of various formulations. The host immune system can eliminate tumor cells by CD8a⁺/CD4⁺ cytotoxic T lymphocytes. CD8a⁺ T cells are the effector cells of tumor-specific immune responses, whereas CD4⁺ T cells help generate CD8a⁺ T cells. In addition, CD4⁺ T cells release pro-inflammatory cytokines, including TNF- α and IFN- γ ^{49,50}. IL-4 is a multifunctional cytokine secreted by the Th2 cells, which has antitumor effects, enhances immune function, and plays an essential role in the development of various tumors⁵¹. BGs stimulated the immune system with a higher level of CD4⁺ T cells in the spleen (Fig. 4F and G), though the level of CD8a⁺ T cells was similar to that of the model mice (Fig. 4F and H). Other studies also show the immune stimulation of BGs^{52,53}. The immune stimulation of BGs was also shown by improvement of the typical pro-inflammatory cytokines, including TNF- α , IL-4, and IFN- γ in the lung, which were higher than those of the model group (Fig. 4I–K). However, our preliminary study showed that a large amount of inhaled BGs led to avoidable deaths due to the strong immune stimulation, so we selected the dose of 25 mg/kg BGs as a safe dose. The immunotherapy and toxicity of BGs are a pair of conflicts, *i.e.*, highly efficient immunotherapy would likely lead to serious toxicity; and by contrast, low toxicity would have no significant immunotherapy. In this study, the BG group did not show enough antitumor effects.

The LP-related immune stimulation was also shown with higher levels of TNF- α and IFN- γ in the lung and CD4⁺ T cells in the spleen than those of the model group (Fig. 3I–G). The LP-killed cancer cells might contribute to the immune stimulation. Other studies also showed similar results^{54,55}. However, the LP-related immune stimulation was weaker than that induced by BGs in all factors. The immune stimulation of LP@BG was stronger than that of BGs and LP, indicating the synthetic effect of

BGs and LP, and possibly resulting from the specific immune action of dead cancer cells and the nonspecific immune action of BGs. Surprisingly, LP@BG@CCM greatly improved immune stimulation compared to the other formulations, which could result from the synergistic result of the components, *i.e.*, CCMs, BGs, and a great number of dead cancer cells.

3.4. High lung biodistribution of LP@BG@CCM

LP@BG@CCM had very high treatment efficiency against metastatic lung cancer, which was related to the strong immune stimulation, and more importantly, the high lung biodistribution of the formulation. We used the fluorescent imaging method to show the biodistribution of carriers. In the whole animal imaging pictures, the fluorescence rapidly disappeared in the free DiR group within 2 h, while both LP@BG@DiR-LM and LP@BG@DiR-CCM maintained the strong fluorescence in the liver and lung for 48 h (Fig. 5A). The fluorescence of excised tissues further showed the biodistribution of carriers. The two carriers, LP@BG@DiR-LM and LP@BG@DiR-CCM, showed strong biodistribution in the liver, lung, and spleen, while free DiR showed a little distribution in these organs (Fig. 5B). The fluorescence intensities in the lung, *i.e.*, metastatic lung tumor tissues, of the groups were very different with the values of 9.56, 49.6, and 124 for free DiR, LP@BG@DiR-LM, and LP@BG@DiR-CCM, respectively. In fact, the fluorescence intensity of the LP@BG@DiR-CCM-treated lung was 2.5 times of that of the LP@BG@DiR-LM-treated lung. The high lung distribution of LP@BG@DiR-CCM may be attributed to the mechanical interception of them by the lung capillaries due to their sizes close to micrometers. Moreover, the homologous affinity function of CCMs may improve the tumor cell internalization of localized LP@BG@DiR-CCM. The homologous affinity effect of CCMs has been widely reported in the literature^{56,57}. In addition, the spleen is the largest immune organ in the body. Immune cells stimulate the body to produce an immune response by capturing bionic bacterial formulations in the peripheral blood⁵⁸. Therefore, the strong lung targeting of LP@BG@CCM benefited to the killing of metastatic lung cancer

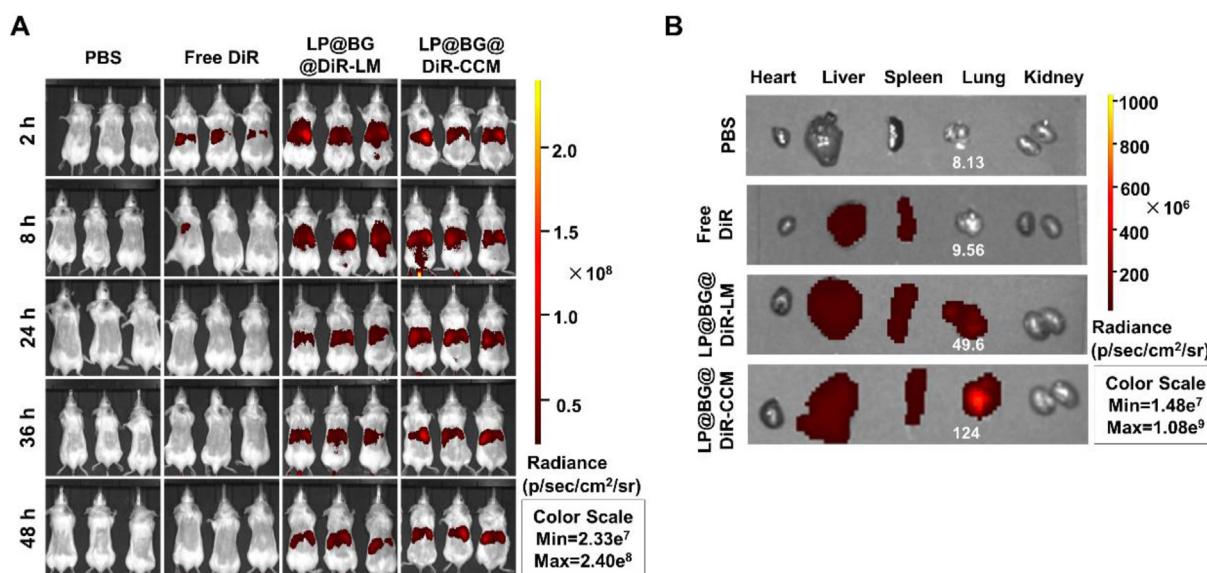


Figure 5 *In vivo* distribution evaluation. (A) Fluorescent images of the metastatic lung tumor-bearing mice and (B) the excised tissues.

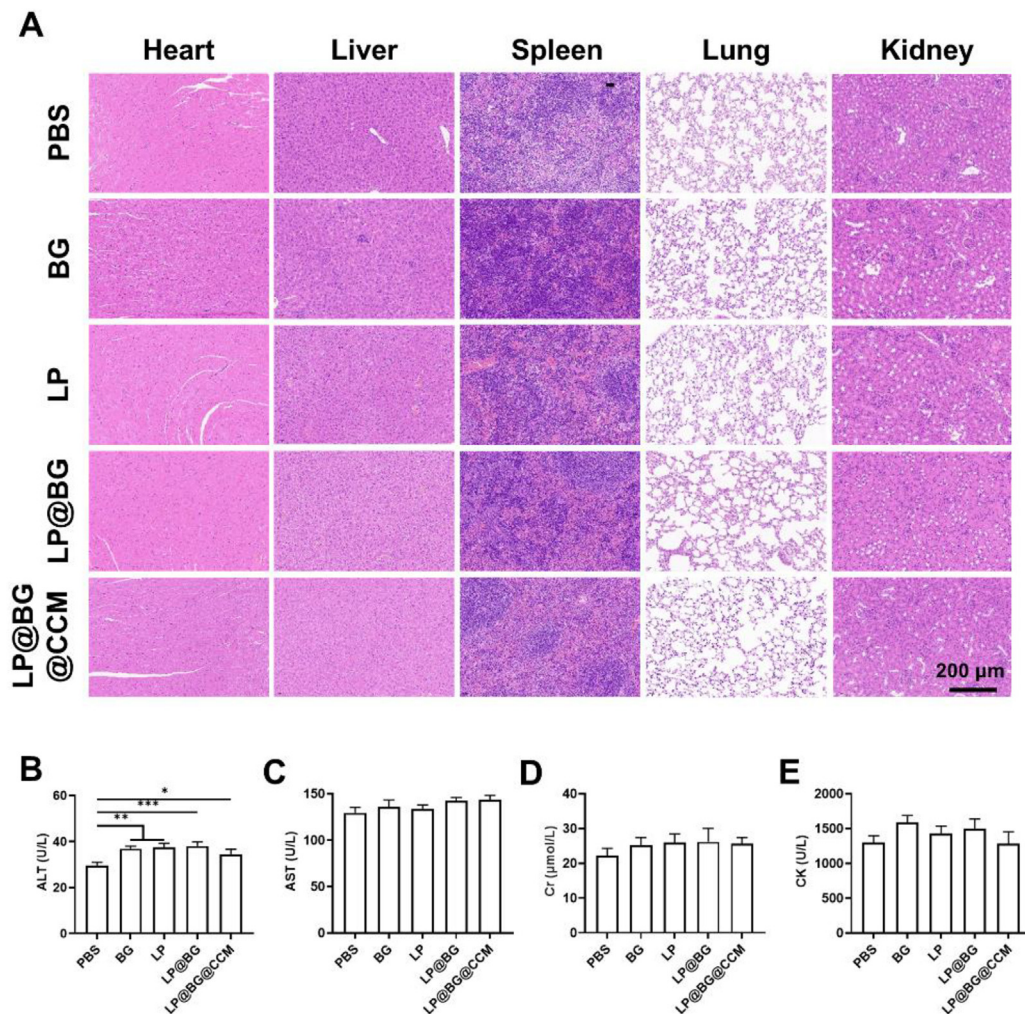


Figure 6 Safety evaluation. (A) H&E images of the tissue sections of various formulations. (B–E) Levels of ALT, AST, Cr, and CK in the serum. Data are presented as mean \pm SD ($n = 3$). * $P < 0.05$, ** $P < 0.01$, *** $P < 0.001$.

cells, and the spleen targeting of LP@BG@CCM benefited to the immune stimulation against metastatic lung cancer.

3.5. High safety of LP@BG@CCM

All the subjects, including PBS, BGs, LP, LP@BG, and LP@BG@CCM, did not affect the structures of the major organ, including the heart, liver, spleen, lung, and kidney after four times of injection (Fig. 6A). The ALT levels of the BGs, LP, LP@BG, and LP@BG@CCM groups were a little higher than the healthy group (Fig. 6B and C), although the levels were in the normal range and the AST levels of all the groups had no statistical difference. Therefore, the liver function basically maintained normal after injection of the formulations. The Cr and CK of all the groups basically maintained the same levels, indicating that the renal and cardiac function was normal (Fig. 6D and E). Therefore, the multiple administration of LP@BG@CCM was safe.

4. Conclusions

Chemotherapy and bacterial immunotherapy of cancer have their advantages and disadvantages. The high doses of them lead to high anticancer effect but strong toxicity; in contrast, the low doses of

them lead to weak anticancer effect though little toxicity. We obtain LP@BG@CCM by layer wrapping simply and efficiently to integrate the advantages of chemotherapy and bacterial immunotherapy but weaken the disadvantages of them to simultaneously achieve high immune stimulation and anticancer effects. Moreover, LP@BG@CCM could have the cascade anticancer function with the release or exposure of CCMs, BGs, and LP in turn to achieve lung targeting, immune stimulation, and cancer cell-killing effects. LP@BG@CCM is a promising anticancer medication for the highly efficient treatment of metastatic lung cancer. More species of Gram-negative bacteria may be also used for the preparation of the synergistic system to achieve specific applications.

Acknowledgements

The work was partially supported by the National Natural Science Foundation of China (81803453).

Author contributions

Dandan Ling, Yiguang Jin and Xueli Jia designed the research, carried out the experiments and performed data analysis. Ke Wang and Qiucheng Yan participated part of the experiments. Bochuang

Yuan and Lina Du directed part of the experiments. Dandan Ling wrote the manuscript. Yiguang Jin revised the manuscript. All of the authors have read and approved the final manuscript.

Conflicts of interest

The authors have no conflicts of interest to declare.

References

- Reck M, Taylor F, Penrod JR, DeRosa M, Morrissey L, Dastani H, et al. Impact of nivolumab versus docetaxel on health-related quality of life and symptoms in patients with advanced squamous non-small cell lung cancer: results from the checkmate 017 study. *J Thorac Oncol* 2018;**13**:194–204.
- Salman B, Al-Khabori M. Applications and challenges in therapeutic drug monitoring of cancer treatment: a review. *J Oncol Pharm Pract* 2021;**27**:693–701.
- Knezevic CE, Clarke W. Cancer chemotherapy: the case for therapeutic drug monitoring. *Ther Drug Monit* 2020;**42**:6–19.
- Lin H, Cheng J, Mu W, Zhou J, Zhu L. Advances in universal CAR-T cell therapy. *Front Immunol* 2021;**12**:744823.
- Lipowska-Bhalla G, Gilham DE, Hawkins RE, Rothwell DG. Targeted immunotherapy of cancer with CAR-T cells: achievements and challenges. *Cancer Immunol Immunother* 2012;**61**:953–62.
- Wu Y, Yang Z, Cheng K, Bi H, Chen J. Small molecule-based immunomodulators for cancer therapy. *Acta Pharm Sin B* 2022;**12**:4287–308.
- Qin SY, Cheng YJ, Lei Q, Zhang AQ, Zhang XZ. Combinational strategy for high-performance cancer chemotherapy. *Biomaterials* 2018;**171**:178–97.
- Huang X, Pan J, Xu F, Shao B, Wang Y, Guo X, et al. Bacteria-based cancer immunotherapy. *Adv Sci* 2021;**8**:2003572.
- Gorjifard S, Goldszmid RS. Microbiota-myeloid cell crosstalk beyond the gut. *J Leukoc Biol* 2016;**100**:865–79.
- Stern C, Kasnitz N, Kocjancic D, Trittel S, Riese P, Guzman CA, et al. Induction of CD4⁺ and CD8⁺ anti-tumor effector T cell responses by bacteria mediated tumor therapy. *Int J Cancer* 2015;**137**:2019–28.
- Pastural É, McNeil SA, MacKinnon-Cameron D, Ye L, Langley JM, Stewart R, et al. Safety and immunogenicity of a 30-valent M protein-based group A streptococcal vaccine in healthy adult volunteers: a randomized, controlled phase I study. *Vaccine* 2020;**38**:1384–92.
- Liang Y, Driscoll AJ, Patel PD, Datta S, Voysey M, French N, et al. Typhoid conjugate vaccine effectiveness in Malawi: evaluation of a test-negative design using randomised, controlled clinical trial data. *Lancet Glob Health* 2023;**11**:136–44.
- Tang Q, Peng X, Xu B, Zhou X, Chen J, Cheng L. Current status and future directions of bacteria-based immunotherapy. *Front Immunol* 2022;**13**:911783.
- Kramer MG, Masner M, Ferreira FA, Hoffman RM. Bacterial therapy of cancer: promises, limitations, and insights for future directions. *Front Microbiol* 2018;**9**:16.
- Thaiss CA, Zmora N, Levy M, Elinav E. The microbiome and innate immunity. *Nature* 2016;**535**:65–74.
- Zhang M, Li M, Du L, Zeng J, Yao T, Jin Y. Paclitaxel-in-liposome-in-bacteria for inhalation treatment of primary lung cancer. *Int J Pharm* 2020;**578**:119177.
- Paukner S, Stiedl T, Kudela P, Bizik J, Al Laham F, Lubitz W. Bacterial ghosts as a novel advanced targeting system for drug and DNA delivery. *Expert Opin Drug Deliv* 2006;**3**:11–22.
- García-Álvarez R, Vallet-Regí M. Bacteria and cells as alternative nano-carriers for biomedical applications. *Expert Opin Drug Deliv* 2022;**19**:103–18.
- Yoo JW, Irvine DJ, Discher DE, Mitragotri S. Bio-inspired, bio-engineered and biomimetic drug delivery carriers. *Nat Rev Drug Discov* 2011;**10**:521–35.
- Won G, Hajam IA, Lee JH. Improved lysis efficiency and immunogenicity of Salmonella ghosts mediated by co-expression of λ phage holin-endolysin and ϕ X174 gene E. *Sci Rep* 2017;**7**:45139.
- Witte A, Wanner G, Sulzner M, Lubitz W. Dynamics of PhiX174 protein E-mediated lysis of *Escherichia coli*. *Arch Microbiol* 1992;**157**:381–8.
- Sheweita SA, Batah AM, Ghazy AA, Hussein A, Amara AA. A new strain of acinetobacter baumannii and characterization of its ghost as a candidate vaccine. *J Infect Public Health* 2019;**12**:831–42.
- Michalek J, Hezova R, Turanek-Knötigova P, Gabkova J, Strioga M, Lubitz W, et al. Oncolysate-loaded *Escherichia coli* bacterial ghosts enhance the stimulatory capacity of human dendritic cells. *Cancer Immunol Immunother* 2017;**66**:149–59.
- Rabea S, Alanazi FK, Ashour AE, Salem-Bekhit MM, Yassin AS, Moneib NA, et al. Salmonella-innovative targeting carrier: loading with doxorubicin for cancer treatment. *Saudi Pharm J* 2020;**28**:1253–62.
- Xie S, Li S, Zhang Z, Chen M, Ran P, Li X. Bacterial ghosts for targeting delivery and subsequent responsive release of ciprofloxacin to destruct intracellular bacteria. *Chem Engineer J* 2020;**399**:125700.
- Salem-Bekhit MM, Youssef AME, Alanazi FK, Aleanizy FS, Abdulaziz A, Taha EI, et al. Bacteria from infectious particles to cell based anticancer targeted drug delivery systems. *Pharmaceutics* 2021;**13**:1984.
- Xie S, Zhao L, Song X, Tang M, Mo C, Li X. Doxorubicin-conjugated *Escherichia coli* Nissle 1917 swimmers to achieve tumor targeting and responsive drug release. *J Control Release* 2017;**268**:390–9.
- Liu Y, Li Z, Wu Y, Jing X, Li L, Fang X. Intestinal bacteria encapsulated by biomaterials enhance immunotherapy. *Front Immunol* 2020;**11**:620170.
- Cao Z, Wang X, Pang Y, Cheng S, Liu J. Biointerfacial self-assembly generates lipid membrane coated bacteria for enhanced oral delivery and treatment. *Nat Commun* 2019;**10**:5783.
- Yao Y, Chen H, Tan N. Cancer-cell-biomimetic nanoparticles systematically eliminate hypoxia tumors by synergistic chemotherapy and checkpoint blockade immunotherapy. *Acta Pharm Sin B* 2022;**12**:2103–19.
- Meng X, Wang J, Zhou J, Tian Q, Qie B, Zhou G, et al. Tumor cell membrane-based peptide delivery system targeting the tumor microenvironment for cancer immunotherapy and diagnosis. *Acta Biomater* 2021;**127**:266–75.
- Zhen X, Cheng P, Pu K. Recent advances in cell membrane-camouflaged nanoparticles for cancer phototherapy. *Small* 2019;**15**:e1804105.
- Zhu JY, Zheng DW, Zhang MK, Yu WY, Qiu WX, Hu JJ, et al. Preferential cancer cell self-recognition and tumor self-targeting by coating nanoparticles with homotypic cancer cell membranes. *Nano Lett* 2016;**16**:5895–901.
- Li A, Zhao Y, Li Y, Jiang L, Gu Y, Liu J. Cell-derived biomimetic nanocarriers for targeted cancer therapy: cell membranes and extracellular vesicles. *Drug Deliv* 2021;**28**:1237–55.
- Rudnick JD, Sarmiento JM, Uy B, Nuno M, Wheeler CJ, Mazer MJ, et al. A phase I trial of surgical resection with gliadel wafer placement followed by vaccination with dendritic cells pulsed with tumor lysate for patients with malignant glioma. *J Clin Neurosci* 2020;**74**:187–93.
- van der Burg SH, Arens R, Ossendorp F, van Hall T, Melief CJ. Vaccines for established cancer: overcoming the challenges posed by immune evasion. *Nat Rev Cancer* 2016;**16**:219–33.
- Miao YQ, Chen MS, Zhou X, Guo LM, Zhu JJ, Wang R, et al. Chitosan oligosaccharide modified liposomes enhance lung cancer delivery of paclitaxel. *Acta Pharmacol Sin* 2021;**42**:1714–22.
- Lv J, Chen L, Zhu Y, Hou L, Liu Y. Promoting epithelium regeneration for esophageal tissue engineering through basement membrane reconstitution. *ACS Appl Mater Interfaces* 2014;**6**:4954–64.
- Cao Z, Cheng S, Wang X, Pang Y, Liu J. Camouflaging bacteria by wrapping with cell membranes. *Nat Commun* 2019;**10**:3452.

40. Zhang X, He S, Ding B, Qu C, Zhang Q, Chen H, et al. Cancer cell membrane-coated rare earth doped nanoparticles for tumor surgery navigation in NIR-II imaging window. *Chem Engineer J* 2020;**385**:123959.
41. Xiao Z, Zhuang B, Zhang G, Li M, Jin Y. Pulmonary delivery of cationic liposomal hydroxycamptothecin and 5-aminolevulinic acid for chemo-sonodynamic therapy of metastatic lung cancer. *Int J Pharm* 2021;**601**:120572.
42. Liu J, Deng Y, Fu D, Yuan Y, Li Q, Shi L, et al. Sericin microparticles enveloped with metal-organic networks as a pulmonary targeting delivery system for intra-tracheally treating metastatic lung cancer. *Bioact Mater* 2021;**6**:273–84.
43. Hajam IA, Dar PA, Appavoo E, Kishore S, Bhanuprakash V, Ganesh K. Bacterial ghosts of *Escherichia coli* drive efficient maturation of bovine monocyte-derived dendritic cells. *PLoS One* 2015;**10**: e0144397.
44. Gutiérrez Millán C, Colino Gandarillas CI, Sayalero Marinero ML, Lanao JM. Cell-based drug-delivery platforms. *Ther Deliv* 2012;**3**: 25–41.
45. Yu Z, Zhou P, Pan W, Li N, Tang B. A biomimetic nanoreactor for synergistic chemiexcited photodynamic therapy and starvation therapy against tumor metastasis. *Nat Commun* 2018;**9**:5044.
46. Sun H, Su J, Meng Q, Yin Q, Chen L, Gu W, et al. Cancer-cell-biomimetic nanoparticles for targeted therapy of homotypic tumors. *Adv Mater* 2016;**28**:9581–8.
47. Zhu Y, Liang J, Gao C, Wang A, Xia J, Hong C, et al. Multifunctional ginsenoside Rg3-based liposomes for glioma targeting therapy. *J Control Release* 2021;**330**:641–57.
48. Liu YH, Liu GH, Mei JJ, Wang J. The preventive effects of hyperoside on lung cancer *in vitro* by inducing apoptosis and inhibiting proliferation through Caspase-3 and P53 signaling pathway. *Biomed Pharmacother* 2016;**83**:381–91.
49. Chen L, Qin H, Zhao R, Zhao X, Lin L, Chen Y, et al. Bacterial cytoplasmic membranes synergistically enhance the antitumor activity of autologous cancer vaccines. *Sci Transl Med* 2021;**13**: eabc2816.
50. Ahrends T, Borst J. The opposing roles of CD4⁺ T cells in anti-tumour immunity. *Immunology* 2018;**154**:582–92.
51. Yu X, Wang L, Yang X, Zhang S, Li G, Zhang L, et al. Lactobacillus casei ghosts as a vehicle for the delivery of DNA vaccines mediate immune responses. *Front Immunol* 2022;**13**:849409.
52. Chen H, Ji H, Kong X, Lei P, Yang Q, Wu W, et al. Bacterial ghosts-based vaccine and drug delivery systems. *Pharmaceutics* 2021;**13**:1892.
53. Dobrovolskienė N, Pašukonienė V, Darinskas A, Kraško JA, Žilionytė K, Mlynska A, et al. Tumor lysate-loaded bacterial ghosts as a tool for optimized production of therapeutic dendritic cell-based cancer vaccines. *Vaccine* 2018;**36**:4171–80.
54. Wang Y, Yu J, Li D, Zhao L, Sun B, Wang J, et al. Paclitaxel derivative-based liposomal nanoplatform for potentiated chemo-immunotherapy. *J Control Release* 2022;**341**:812–27.
55. Xiao Y, Zhang T, Ma X, Yang QC, Yang LL, Yang SC, et al. Microenvironment-responsive prodrug-induced pyroptosis boosts cancer immunotherapy. *Adv Sci* 2021;**8**:e2101840.
56. Allami P, Heidari A, Rezaei N. The role of cell membrane-coated nanoparticles as a novel treatment approach in glioblastoma. *Front Mol Biosci* 2022;**9**:1083645.
57. Fang RH, Hu CM, Luk BT, Gao W, Copp JA, Tai Y, et al. Cancer cell membrane-coated nanoparticles for anticancer vaccination and drug delivery. *Nano Lett* 2014;**14**:2181–8.
58. Fan Y, Cui Y, Hao W, Chen M, Liu Q, Wang Y, et al. Carrier-free highly drug-loaded biomimetic nanosuspensions encapsulated by cancer cell membrane based on homology and active targeting for the treatment of glioma. *Bioact Mater* 2021;**6**:4402–14.